Aeolian dune field geomorphology modulates the stabilization rate imposed by climate

Thomas E. Barchyn[1] and Chris H. Hugenholtz[1,2]

[1]   The activity of inland aeolian dune fields is typically related to the external forcing imposed by climate: active (bare) dunes are associated with windy and/or arid settings, and inactive (vegetated) dunes are associated with humid and/or calm environments. When a climate shifts the dune field reacts; however, the behavior, rate, and potential impact of diverse dune geomorphologies on these transitions are poorly understood. Here, we use a numerical model to systematically investigate the influence of dune field geomorphology (dune height, organization and collisions) on the time a dune field takes to stabilize. To generate diverse initial un-vegetated dune field geomorphologies under unidirectional winds, we varied pre-stabilization growth time and initial sediment thickness (termed equivalent sediment thickness: EST). Following dune field development from a flat bed, we introduced vegetation (simulating a climate shift) and transport-vegetation feedbacks slowly stabilized the dune fields. Qualitatively, very young and immature dune fields stabilized quickly, whereas older dune fields took longer. Dune fields with greater EST stabilized quicker than those with less EST. Larger dunes stabilized quicker because of low celerity, which facilitated higher vegetation growth rates. Extended stabilization times were associated with the extension of parabolic dunes. Dune-dune collisions resulted in premature stabilization; the frequency of collisions was related to dune spacing. Quantitatively comparing the distribution of deposition rates in a dune field to the deposition tolerance of vegetation provides a promising predictor of relative stabilization time. Dune fields with deposition rates dominantly above the deposition tolerance of vegetation advanced unimpeded and prolonged stabilization as parabolic dunes. Paleoenvironmental reconstructions or predictions of dune field activity should not assume that dune activity directly translates to climate, considerable lags to stabilizing climate shifts may exist in unidirectional dune forms.

1.   Introduction

[2]   Many inland dune fields transition between active (mobile) and stabilized (vegetated) states. Two aspects of climate are generally thought to control temporal transitions: i) wind speed, which drives sediment transport, and ii) aridity, which controls vegetation growth rate [*Lancaster*, 1988; *Hugenholtz and Wolfe*, 2005a, 2005b; *Tsoar*, 2005; *Yizhaq et al.*, 2007, 2009]. Arid and/or windy environments are commonly associated with bare, active dunes. Humid and/or calm environments typically result in stabilized dunes.

In general, these variables are considered as a ratio of sediment transport potential to aridity. For example, dunes in windy and humid environments can have similar activity to those in calm and arid environments [*Ash and Wasson*, 1983; *Lancaster*, 1988].

[3]   Dune fields can be exceedingly sensitive to climate variability; many have undergone repeat transitions between activity and stabilization multiple times [*Thomas and Wiggs*, 2008]. Presently, some dune fields are observably in transition [e.g., *Tsoar and Blumberg*, 2002; *Ardon et al.*, 2009] (see Figure 1) or are still responding to climate shifts hundreds of years in the past [e.g., *Hugenholtz and Wolfe*, 2005b; *Wolfe and Hugenholtz*, 2009, Figure 1]. In the future, climate changes could result in consequential activity changes [e.g., *Thomas et al.*, 2005]. Semi-arid regions most susceptible to changes in dune field activity also tend to be the most inhabited of dune lands; therefore, understanding the controls on dune field activity has implications for socio-economic adaptation.

[4]   Although a simple time-independent relation between climate and dune activity is an attractive and widely used

[1]Department of Geography, University of Lethbridge, Lethbridge, Alberta, Canada.
[2]Faculty of Environmental Design, University of Calgary, Calgary, Alberta, Canada.

Corresponding author: T. E. Barchyn, Department of Geography, University of Lethbridge, 4401 University Drive, Lethbridge, AB T1K 3M4, Canada. (tom.barchyn@uleth.ca)
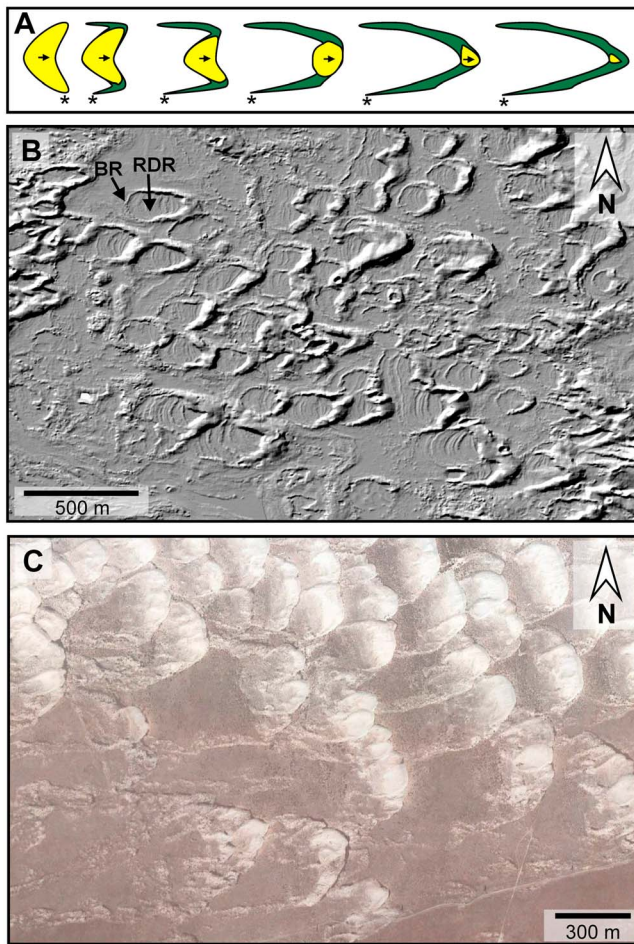
Figure 1. Examples of dune stabilization. (a) Conceptual understanding of the transition between barchan and parabolic dunes: arms vegetate first and become immobile while the center of the dune advances downwind before stabilizing (the asterisk marks an immobile point of reference). (b) Hillshade image revealing morphological remnants of the barchan-parabolic transformation [see *Wolfe and Hugenholtz*, 2009], including back ridges (BR), residual dune ridges (RDR) (image centered on 50.2161° N, 109.2279° W). (c) Stabilizing parabolic dunes at Hanford Nuclear Reservation, Hanford, WA, USA. Dunes are migrating from left to right, image centered on 46.4953° N, 119.2907° W (Google Earth imagery © Google Inc. Used with permission).

model [e.g., *Ash and Wasson*, 1983; *Lancaster*, 1988; *Bullard et al.*, 1997], in reality there is some period of transition between states [*Bullard et al.*, 1997; *Tsoar*, 2005; *Hugenholtz and Wolfe*, 2005a, 2005b; *Yizhaq et al.*, 2007, 2009]. Very little is known about the rate or process of dune field activity transitions beyond basic observation [*Bullard et al.*, 1997], inferences made with relatively simple differential equations [*Hugenholtz and Wolfe*, 2005a; *Yizhaq et al.*, 2007, 2009] and a series of simulation studies by *Nield and Baas* [2008a, 2008b]. The latter studies revealed considerable complexity in activity transitions of simulated dune fields and indicated that behavior in transitions may be intricately linked to dune field history and geomorphology. Understanding of transitions is important because climate is

not static; inland dune fields can be envisioned to constantly lag behind a given climate. Lag times could explain observed cases where dune fields are out of sync with present climate [*Yizhaq et al.*, 2007, 2009].

[5] Despite limited understanding of activity transitions, there has been widespread use of dune activity as a proxy for paleoaridity, spurred by improved luminescence dating technology [e.g., *Forman et al.*, 2001; *Chase and Thomas*, 2006; *Miao et al.*, 2007; *Stone and Thomas*, 2008; *Wolfe et al.*, 2011]. These proxies of aridity are subsequently applied to advance understanding of global climate systems and improve global climate models [*Chase*, 2009]. Many researchers acknowledge that extrapolation of paleoaridity from dune activity records is limited by poor understanding of contemporary dune activity [*Bullard et al.*, 1997; *Hugenholtz and Wolfe*, 2005a; *Chase*, 2009].

[6] To gain greater insight into the process of dune field stabilization, it would be helpful to make direct observations. Unfortunately, dune field stabilization occurs on longer timescales than most remote sensing or scientific records. Only a few multitemporal records are available that document *portions* of stabilization of a *few* isolated dune fields [*Pye*, 1982; *Anthonsen et al.*, 1996; *Tsoar and Blumberg*, 2002; *Bailey and Bristow*, 2004; *Hugenholtz and Wolfe*, 2005b; *Marín et al.*, 2005]. Larger scale dune chronologies tend to emphasize the extremes of dune activity states: either active or stabilized; they provide little indication of the transition between these states. However, recent advances in numerical modeling are now providing insight into unobservable stabilization processes. With numerical models, centuries of dune field evolution can be run in a matter of minutes and repeated with slightly different parameters hundreds of times [e.g., *Durán and Herrmann*, 2006; *Nield and Baas*, 2008a, 2008b].

[7] Here, we follow this approach; we use a simple numerical model to examine the behavior of a stabilizing dune field. We limit the scope to a simple case: a closed-system inland dune field under a unidirectional wind. Specifically, we focus on the time a dune field takes to stabilize under variable pre-stabilization geomorphology. This can be described as the 'stabilization lag time' for a dune field [*Hugenholtz and Wolfe*, 2005a].

[8] Un-vegetated dune fields under a unidirectional wind vary in their geomorphology. Throughout this manuscript, we use the word 'geomorphology' to describe i) the general morphology of dunes in the dune field, and ii) the kinematics of dunes. Qualitative elements of dune field geomorphology under a unidirectional wind are well understood in both empirical [*Ewing et al.*, 2006; *Ewing and Kocurek*, 2010a, 2010b; *Kocurek et al.*, 2010] and simulated contexts [*Werner*, 1995; *Eastwood et al.*, 2011]. In general, dunes grow in height from a flat bed with growth time; however, it is unclear if dunes ever reach some stable 'steady state' size [cf. *Pelletier*, 2009; *Diniega et al.*, 2010; *Ewing and Kocurek*, 2010b]. The quantity of sediment present in a dune field also controls morphology; this is typically quantified with a concept known as equivalent sediment thickness (EST), which is defined as the thickness of sediment that would result if all dunes were flattened [*Wasson and Hyde*, 1983]. Dune fields with greater EST typically form transverse dunes; dune fields with less EST break apart into barchan dunes [*Wasson and Hyde*, 1983]. However, it is
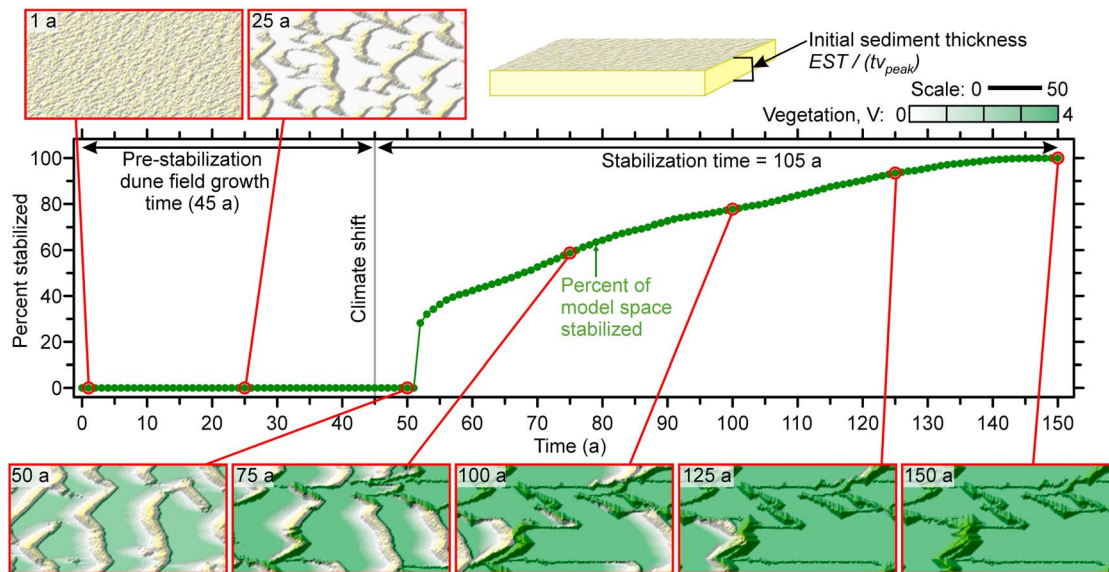
Figure 2.   An example of the simulations used in this study. Dune fields were initiated with a thickness of sediment equivalent to scaled measurement ($EST/(tv_{peak})$; see equation (1)). Dune fields started without vegetation and were run forward without vegetation for a time interval representing the pre-stabilization dune field growth time. Vegetation was introduced with a climate shift (at 45 a in this simulation). The dune field subsequently began stabilizing and eventually stabilized 105 a after the climate shift. The equivalent sediment thickness of this simulation was 0.5 and vegetation was grown with growth curve C1 (see Figure 3). The percent stabilized refers to the percent of the model space where vegetation has reached the maximum value in the model ($V = 4$). The sharp jump in percent of model space stabilized after the climate shift is due to the interdune areas which take 8 a to grow to the maximum value.

important to note that there is a continuum of dune connectivity between barchan and transverse dunes. The downwind advance (celerity) of dunes in a dune field is inversely correlated with their height [*Bagnold*, 1941]: larger dunes travel slower than smaller dunes. Given this diversity of un-vegetated dune behavior (e.g., growth time, connectivity, celerity), one could expect different dune fields to respond differently to the introduction of vegetation.

[9] To simulate stabilization under different dune field geomorphologies, we started the model with a flat bed and no vegetation. The model was run with a variety of initial sediment thicknesses (EST) and pre-stabilization growth times to generate a variety of dune field geomorphologies, from small immature dunes to large barchan and transverse dunes. We systematically stabilized the dune fields by introducing vegetation with one of two vegetation growth regimes (see Figure 2). Throughout, we hold sediment transport and vegetation growth regime constant. Gradually, feedbacks between vegetation and sediment transport stabilized the dunes. In some cases, stabilization converted the dunes from barchan or transverse dunes to parabolic dunes. We found substantial variability in stabilization time that can be attributed to the geomorphology of the dune field. We outline the potential significance of the simulation results in the context of paleoenvironmental reconstruction and prediction of dune field activity.

2. Model Algorithm

[10] Our Biomorphodynamic Aeolian Model (BAM) is closely related to other vegetated dune models [*de Castro*,

1995; *Nishimori and Tanaka*, 2001; *Baas*, 2002, 2007; *Durán and Herrmann*, 2006; *Baas and Nield*, 2007; *Nield and Baas*, 2008a, 2008b; *Pelletier et al.*, 2009; *de M. Luna et al.*, 2011]. It is pertinent to note that a dearth of multi-century vegetation cover and topography data limits our capacity to quantitatively validate model outputs. As such, similar to other vegetated dune models [e.g., *Durán and Herrmann*, 2006; *Baas and Nield*, 2007], outputs from the BAM should be considered hypotheses rather than quantitative predictions of actual dune field stabilization outcomes. Despite this caveat, our vegetated dune model produces qualitatively realistic-looking un-vegetated and vegetated dunes, suggesting that it has captured the basic feedbacks and mechanisms present in inland dune systems.

[11] We use a non-dimensional spatial scale in our model to avoid site specificity and facilitate preliminary quantitative comparison of our simulations with real dunes. We scale model space with the peak deposition tolerance of vegetation (v_{peak}) and the time used to measure v_{peak} (t):

$$l_{real} = l_{model} \cdot tv_{peak} \; with \; limits \; for \; v_{peak} \approx [0.5, 3.0] \, \mathrm{m \, a^{-1}} \quad (1)$$

where l_{real} and l_{model} are length measurements in the real and model world, respectively. Note that for convenience we use a time scale (t) of years throughout the manuscript, in both modeled and real contexts; as such, t is constant at 1 a. As v_{peak} is a rate (units: m a^{-1}), lengths in the model are scaled with tv_{peak} (equation (1)). In effect, this scaling locks spatial and temporal scale to the characteristics of vegetation (following *Baas and Nield* [2007]). Note: there are limits to realistic values of v_{peak} that our simulations

will represent due to our fetch parameterization, which does not scale over a wide range without assuming unrealistic values; this is discussed further in subsequent paragraphs. A note on Notation: where defined, we use capital letters to denote model values (e.g., H), and lowercase variable names (e.g., h) to denote real measurements (see Notation).

[12] The BAM incorporates simple representations of five basic mechanisms: i) downwind sediment transport, which is limited in lee shadow zones; ii) avalanching at the angle of repose; iii) vegetation growth and death controlled by topographic change; iv) reduced sediment transport in the presence of vegetation; and v) a fetch algorithm that reduces sediment transport based on upwind distance to the un-vegetated patch boundary. We follow the simulation philosophies of *Werner* [1995] and *Murray* [2007], wherein we deliberately keep the model simple to improve understanding of the resultant complex behavior.

[13] The model space consists of 3 arrays: surface height (H), non-erodible basement (B), and vegetation effectiveness (V; hereafter referred to as 'vegetation'). All boundaries are periodic. Vegetation effectiveness is a measurement of the ability for vegetation to reduce surface shear stress, conceptually analogous to the frontal area index of vegetation elements. We scale vegetation to the value that results in complete cessation of transport ($v_{shelter}$) ($\approx$15% surface cover [e.g., *Wasson and Nanninga*, 1986; *Lancaster and Baas*, 1998]). This sets real vegetation cover (v) to $V \cdot v_{shelter}$ and closely follows *Baas and Nield* [2007]. Shear stress from the wind (τ) is constant across the model space ($\tau = 1$) and reduced linearly by vegetation where effective shear stress is equal to $\tau_{i,j} - V_{i,j}$ at each site with coordinates of i, j. Shear stress is completely eliminated ($\tau_{i,j} = 0$) if the site is in a lee shadow zone. Lee shadow zones are cells that fall below a 15° line traced downwind from every high point (following *Werner* [1995]); this simulates the zone of airflow separation in the lee of dunes [*Frank and Kocurek*, 1996]. The algorithm has the advantage of being simple to understand, straightforwardly applicable to large dune fields [*Baas and Nield*, 2010], and computationally efficient enough to allow simulation of thousands of dune fields. The surface height can vary to any value where $H > B$; B is locked at 0. We limit the range of V between 0 and 4, simulating the common situation in dune environments where vegetation continues growing after sediment transport is ceased [*Lancaster and Baas*, 1998]. Contrary to the model of *Nield and Baas* [2008a, 2008b], V cannot drop below 0. When the topography between a cell and one of its four cardinal neighbors exceeds the angle of repose (34°), the model moves sediment downhill from the highest cell until the slope is equal to the angle of repose. In the rare case where the steepest slope is identical between two of the neighbors, the model picks one randomly. Avalanches recursively propagate up or down slopes to ensure all cells have slopes less than the angle of repose.

[14] Streamwise sediment flux (Q) is limited near upwind boundaries, simulating a fetch effect. *Delgado-Fernandez* [2010] compiled empirical estimates and models of the fetch effect and found: i) fetch effects are real and important, ii) estimates range from a few meters to a few hundred meters, iii) a summary of models suggests transport increases approximately linearly from an upwind boundary [see *Delgado-Fernandez*, 2010, Figure 2] to a critical fetch

distance (D_{fetch}), and iv) the fetch effect is the result of a number of different sub-processes, for example, surface moisture [*Nield*, 2011].

[15] Given this considerable uncertainty, we conservatively assume fetch increases linearly and is approximately scaled where $D_{fetch} = 10$ cells, which is a real distance of $10 \cdot tv_{peak}$. If v_{peak} ranges from 0.5 to 3.0 m a^{-1}, this gives real fetch distances ranging from 5 to 30 m, which is within the range of estimates presented by *Delgado-Fernandez* [2010]. In the BAM, we compute sediment flux in a linear addition algorithm: fetch is added in a 'while' loop that adds flux to a running total with distance upwind (D_{upwind}) from a focal cell to D_{fetch}, where flux reaches the maximum flux value (Q_{max}). The edge of exposed fetch for a bare and active sand patch can exist when: i) there is no sediment, ii) the site is in a lee shadow zone ($\tau = 0$), or iii) the local vegetation value ($V_{i,j}$) completely eliminates transport ($V_{i,j} > 1$) with

$$Q = \sum (\tau_{i,j} - V_{i,j}) Q_{max} / D_{fetch} \ from \ D_{upwind} = 0 \ to: (\tau_{i,j} - V_{i,j}) \leq 0 \ or$$
$$H_{i,j} = 0 \ or$$
$$D_{upwind} = D_{fetch} \qquad (2)$$

where each iteration of the lop increments the D_{upwind} counter 1. Similar fetch effects are incorporated into the model of *Baas and Nield* [2007] by modifying the probabilities for erosion of slabs in vegetated cells, and by *Durán and Herrmann* [2006] as a flux saturation calculation. The primary effect of the fetch effect is an improvement of the parabolic arm morphology by reducing the size of patches that can sustain downwind movement. An example of a stabilized dune field without the fetch effect is given in the auxiliary material (Animation S4).[1]

[16] The model proceeds through time by picking a random location in the model space, calculating Q, and moving Q sediment 1 cell downwind. One 'iteration' of time occurs after the model has performed the same number of transport events as the number of cells in the model space. One year equals 100 iterations. Q_{max} is held constant throughout all simulations with $Q_{max} = 0.1$ per transport event. For an arbitrarily scaled model we can approximate the real yearly sediment flux (q_{max}) with

$$q_{max} \approx 100 \cdot Q_{max} (tv_{peak})^2 \qquad (3)$$

where q_{max} is in units of m^2 a^{-1}. The 100 constant in equation (3) is required to convert Q_{max}, which is expressed per model transport event, to a value per year. In non-dimensional model units, this results in a bulk yearly transport of 10 a^{-1}. Note that we have iteratively chosen the value of Q_{max} to match our vegetation growth curves (Figure 3) and produce a realistic range of simulation outcomes. Although our simulations can be arbitrarily scaled, the simulations can only be directly compared with reality if a similar sediment flux occurs, as calculated with equation (3).

[17] Vegetation growth rate is calculated once every year as a function of the net topographic change during the

---

[1]Auxiliary material data sets are available at ftp://ftp.agu.org/apend/jf/ 2011JF002274. Other auxiliary material files are in the HTML. doi:10.1029/2011JF002274.
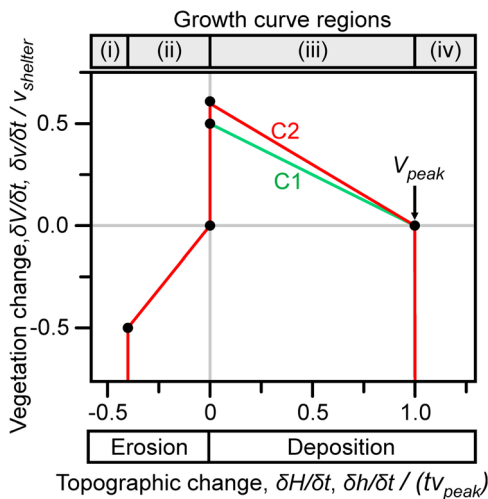
Figure 3. Growth curve regimes used to stabilize dune fields. The growth curve regions are described in the text. At the end of each time interval t, the model calculates the change in vegetation at a site by first calculating topographic change (bottom axis), and then determining the vegetation change (left axis). Both topographic and vegetation change can be expressed in model or real units (see text for Notation). The peak deposition tolerance of vegetation is referred to as V_{peak} and is used to scale the model (see equation (1)).

previous year with one of two growth curves: C1 or C2 (similar to *Baas and Nield* [2007]) (see Figure 3). We simulate two different growth curves to investigate the consistency of results under two different climate forcings. This simulates seasonal vegetation growth similar to the type that occurs on the Canadian Prairies, where vegetation growth occurs during a short time in early summer when winds are calm [see *Hugenholtz*, 2010]. Vegetation growth at a site is calculated by first checking the topographic change over the previous year (bottom axis, Figure 3), and then adding the corresponding quantity of vegetation (left axis, Figure 3) to the total at the site. We incorporate 4 descriptive zones of characteristic vegetation response into the model: i) extreme erosion: all vegetation is excavated and removed, ii) minor erosion: vegetation eroded and removed through decomposition on the dune surface, iii) minor deposition: vegetation grows at maximum rate, and iv) extreme deposition: all vegetation is buried. These zones qualitatively match vegetation growth characteristics described by *Brown* [1997], *Maun* [1998], *Maun and Perumal* [1999], *Franks and Peterson* [2003], and *Owen et al.* [2004]. The sharp difference in growth rate seen between zones (ii) and (iii) is poorly researched [*Bowers*, 1982], but is widely seen on real parabolic dunes. For example, most parabolic dunes do not support vegetation growth on the stoss slope [*Pye*, 1982; *Durán et al.*, 2008; *Hugenholtz*, 2010]. Stoss slopes have generally shallow gradients and thus, for a given celerity, have relatively low erosion rates; the lack of vegetation growth in this region of dunes suggests that vegetation is exceedingly intolerant to erosion. If deposition enters zone (iv) between yearly vegetation adjustments, vegetation is immediately buried ($V_{i,j} = 0$), simulating an advancing slipface [*Dech and Maun*, 2005].

[18] Our growth curves are necessarily simplistic. The response of vegetation growth to topographic change has only been parameterized for isolated species, and only for deposition of sand [e.g., *Maun*, 1998]. Furthermore, often these studies only measure biologically relevant aspects of plant growth such as biomass or seed survival. This information is not possible to reliably translate into a reduction of near surface shear stress, a parameter required by the model. By following previous works [*Durán and Herrmann*, 2006; *Baas and Nield*, 2007, 2010; *Nield and Baas*, 2008a, 2008b] we use growth curves that qualitatively match expected growth tolerances. However, it is important to note that different vegetation types or species could vary in response to topographic change [e.g., *Zarnetske et al.*, 2012]; thus, our results are specific to a growth curve that approximately follows Figure 3. We use a nonlinear growth curve because vegetation growth is widely acknowledged to vary as a function of topographic change (e.g., deposition stimulation) [*Maun*, 1998; *Maun and Perumal*, 1999]. Simpler approaches that rely on a one number 'vegetation growth' measured as vertical growth rate of vegetation elements [e.g., *Durán and Herrmann*, 2006] could approximate v_{peak} with the 'vegetation growth rate'. Finally, it is important to note that although we refer to the introduction of vegetation as a 'climate shift', similar changes in the growth regime of vegetation could result from other situations, such as introduction of non-native invasive species [e.g., *Zarnetske et al.*, 2012], or changes to the hydrogeological regime [e.g., *Laity*, 2003].

3. Simulations

[19] The purpose of the simulations was to examine systematic differences in the time that a dune field takes to stabilize under different un-vegetated dune field geomorphologies. We held the vegetation growth parameters and sediment flux constant throughout all simulations.

[20] All simulations were initialized with a model space 100 cells cross-wind by 200 cells downwind, composed of a flat bed of erodible cells with a depth equivalent to the specified equivalent sediment thickness (EST). Dunes were allowed to evolve for a measured interval of time without vegetation (representing pre-stabilization growth time) before the climate was shifted to introduce vegetation (to either C1 or C2 growth curves; see Figures 2 and 3). Results were output in yearly intervals. We simulated two different growth curves to investigate the consistency of results.

[21] We simulated 5 replicates of 300 unique parameter combinations, which were developed from combinations involving: i) two growth regimes (Figure 3), ii) 15 values of pre-stabilization dune field growth time (5–75 a at 5 a increments), and iii) 10 values of *EST* (0.5–2.75, intervals of 0.25 model length units). Due to randomness in the ordering of transport events each simulation was unique. Stabilization time was measured by differencing the time from the introduction of vegetation to when 100% of the model space had $V = 4$, representing complete dune field stabilization and cessation of any changes in the model space. Ranges in stabilization time were calculated by subtracting the maximum and minimum stabilization times within the 5 replicates. Dune height was approximated for the entire dune field by subtracting the 90% and 10% quantiles of H. With
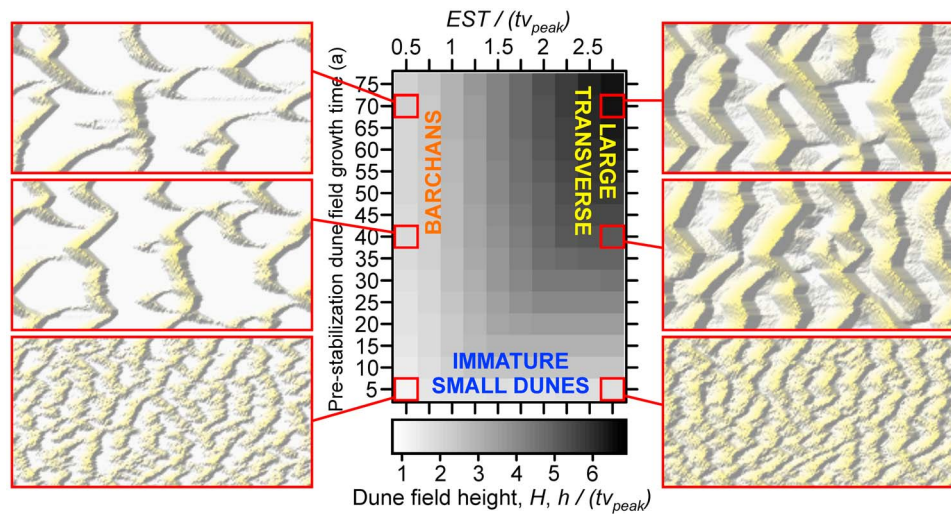
Figure 4. Pre-stabilization geomorphology of dune fields. Increasing the pre-stabilization growth time and equivalent sediment thickness (*EST*) results in taller dunes, which are typically composed of large transverse dunes. Height can be expressed in both real and model units (see Notation and equation (1)). The goal of our study is to examine how these diverse dune field geomorphologies behave with the introduction of vegetation.

periodic boundaries, no sediment leaves or enters the system, thus the initial thickness of sediment in the model space is equivalent to the final EST.

[22] Although we have scaled the simulated dunes with tv_{peak}, which yields dunes that could theoretically be compared with any dune field, it is important to note that the simulations we show are specific to the value of Q_{max} (0.1 per transport event). We iteratively chose this value to: i) develop dune fields in a reasonable amount of time, ii) balance with growth curves C1 and C2 to produce a variety of stabilization behaviors, and iii) match transport rates of $\approx$40 m^2 a^{-1} if $v_{peak} \approx 2$ m a^{-1}, simulating an active aeolian environment with strong vegetation growth like that experienced in the Canadian Prairies [*Hugenholtz et al.*, 2009; *Hugenholtz*, 2010].

4. Results

[23] Prior to the introduction of vegetation, simulated dunes rapidly increased in size from a flat bed. Mergers between incipient bed forms increased the organization, size, height (see Figure 4), and spacing of dune forms (similar to *Werner* [1995], *Kocurek et al.* [2010], *Bo and Zheng* [2011], and *Eastwood et al.* [2011]. We draw no difference between transverse and barchans dunes and consider the two forms in a continuum. To clarify semantics we use the term 'crest termination' to describe the end of a brinkline (as defined by *Werner* [1995]). Isolated barchans have 2 crest terminations per dune form, and transverse dunes have fewer, depending on the connectivity of the dunes. The number of crest terminations decreased through time during dune field construction, similar to results by *Eastwood et al.* [2011].

[24] The variability in EST and pre-stabilization dune field growth time produced a variety of different dune configurations. Dune fields with greater pre-stabilization growth time and less EST had wider-spaced dunes. Dune height

increased with EST and pre-stabilization growth time (Figure 4). Dune field organization increased with pre-stabilization growth time. All simulations eroded to the non-erodible basement.

[25] With the introduction of vegetation all simulated dunes swiftly responded to the increased vegetation growth rate (see Figures 2 and 5 and Animations S1–S3). Vegetation in interdune areas rapidly grew due to minimal erosion and deposition. On active sand, crest terminations were the first part of dunes to vegetate (example marked with blue circle in Figure 5b). Vegetation anchored the crest terminations and the center of some dunes moved forward, representing a shift from barchan or transverse morphology ('horns' pointing downwind) to parabolic ('arms' trailing upwind).

[26] Under a C1 vegetation growth regime, most moderate and small-sized dunes completed the transition to a parabolic form (Figure 5) and extended downwind at a distance roughly proportional to their size. Very small transverse dunes that transformed to parabolic dunes extended downwind for a short distance before stabilizing by losing sediment to trailing arms. Larger parabolic dunes were more likely to collide with other dunes downwind. The number of dune-dune collisions increased as parabolic dunes extended further before stabilizing (example marked with red arrow in Figure 5b). Under a C2 growth regime, most of the same characteristics were observed; however, dunes stabilized quicker due to the increased vegetation growth rate. Comparing the two climate shifts, stabilization times under the C1 climate shift were almost twice as long as stabilization under the C2 shift (Figure 6) due to the lower vegetation growth rate. Systematic differences are present within each group; these differences form the focus of this study (Figure 6).

[27] Both C1 and C2 growth curves produced dune fields with consistent stabilization behavior. Under conditions of low EST dune fields with greater pre-stabilization growth
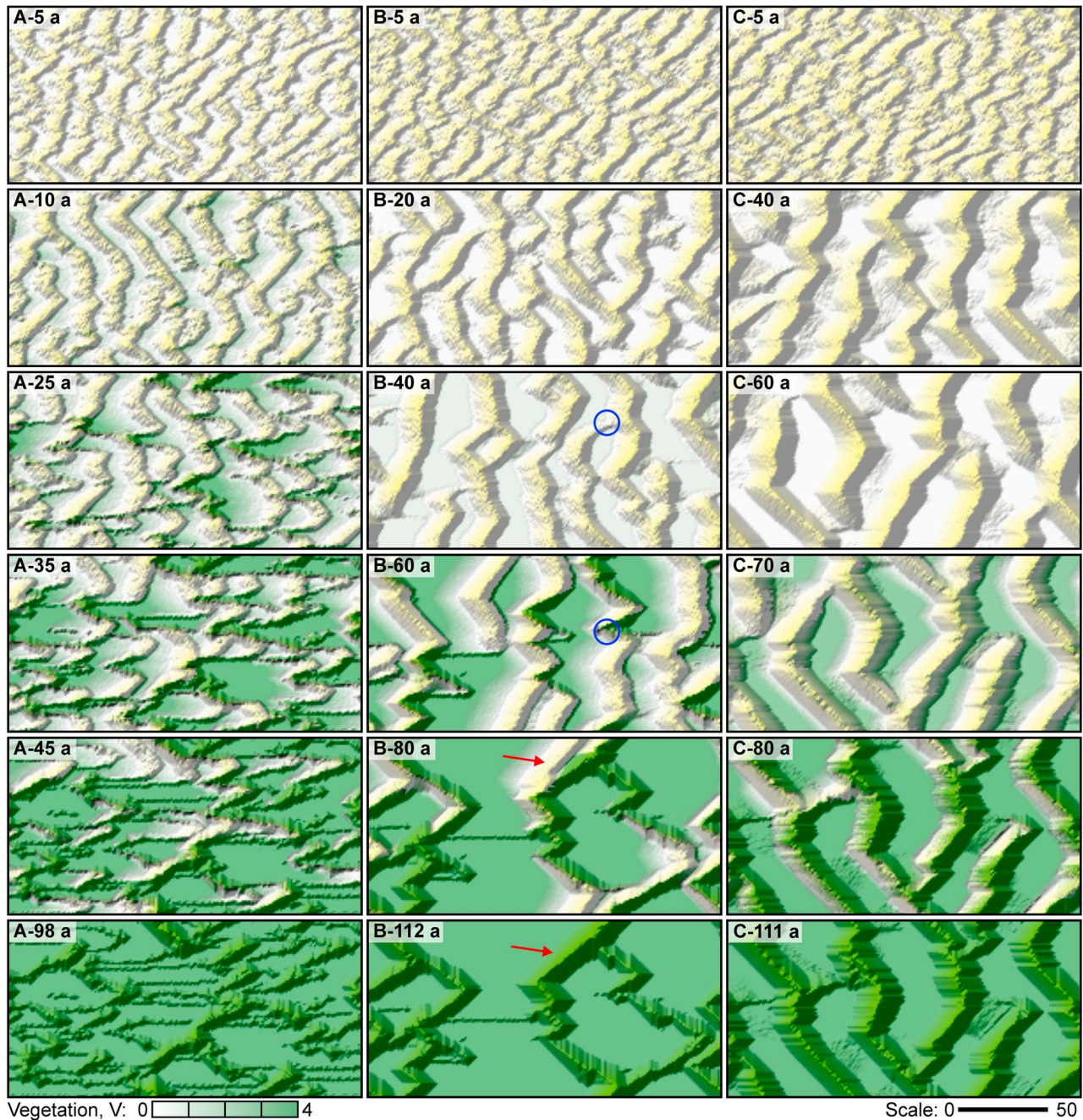
Figure 5. Sample simulation images. (a) Stabilization of an immature and young dune field with equivalent sediment thickness of $EST/(tv_{peak}) = 0.75$ and pre-stabilization growth time of 10 a. (b) Stabilization of a moderate sized dune field with prolonged stabilization, $EST/(tv_{peak}) = 1.25$, pre-stabilization growth time = 40 a. Blue circle: example of a crest termination that preferentially stabilized. Red arrow: an example of a dune-dune collision. (c) Stabilization of a large transverse dune field, $EST/(tv_{peak}) = 2.25$, pre-stabilization growth time = 65 a. Wind is from left to right, all boundaries are periodic, dunes that migrate off the right side of the model space re-appear on the left side. Full animations of these simulations are available as auxiliary material (Animations S1–S3); data summaries of these simulations are also given in the auxiliary material (Data Sets S1–S3).

time took longer to stabilize than those with less pre-stabilization growth time. Under conditions of greater EST the relation was reversed but not as prominent; dune fields with less pre-stabilization growth time took longer than those with greater pre-stabilization growth time. In general,

longer stabilization times occurred with lower EST. The longest stabilization times occurred in dune fields with moderate EST and moderate pre-stabilization growth time (≈45 a) (see Figure 6). With this combination, dunes started small (fast) and transitioned fully to the parabolic
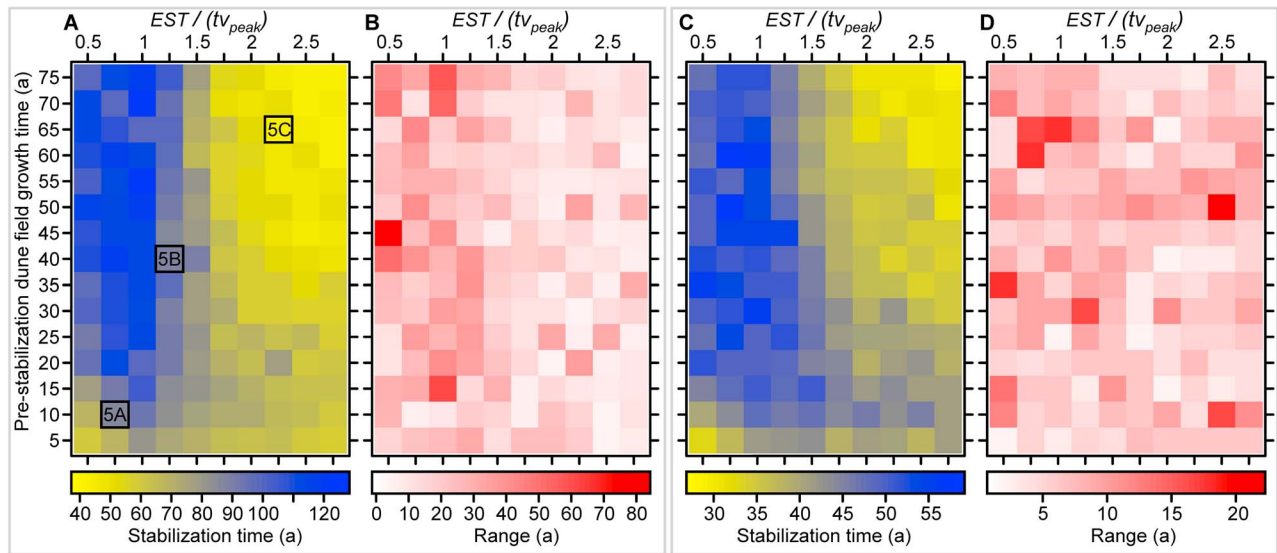
Figure 6. Systematic differences in the stabilization time (defined in Figure 1) occurred with different dune field geomorphologies (see Figure 4). Note that the vegetation growth regime and sediment transport was held constant. (a) Mean of 5 replicates for climate shift C1, and (b) range. (c) Mean of 5 replicates for climate shift C2, and (d) range.

morphology, prolonging stabilization. Also, lower quantities of EST increased inter-dune spacing and allowed dunes to extend further without colliding. Both climates showed variability in stabilization time (shown as ranges in Figures 6b and 6d); however, the general trends are consistent.

5. Discussion

[28] There were pronounced differences in the stabilization rates of simulated dune fields; in some instances dune fields under a different EST or pre-stabilization growth time took twice as long to stabilize (Figure 6). These differences were brought about by markedly different dune geomorphology at the instance vegetation was introduced (Figure 4). The influence of EST and pre-stabilization growth time has a number of predictable effects on the evolution of bare dune fields once stabilization begins.

[29] We first discuss the model and simulation strategy before exploring qualitative behaviors that are helpful to understand the results. Finally, we describe a quantitative method that could be used to predict stabilization times of real dune fields. Please note: in this section we refer to *simulated* dunes unless otherwise noted.

5.1. Modeling and Simulation Strategy

[30] Although the BAM is based on very simple linear relations between parameters, the basic feedbacks present in dune environments are effectively represented. Modeled dunes lack some of the subtle detail that real dunes have (e.g., residual dune ridges; see Figure 1) [*Wolfe and Hugenholtz*, 2009]. Modeled dunes also tend to show more 'angular' morphologies than would be expected in real dunes. This is partly the result of the simple model structure and partly due to the simplified simulation strategy. For example, parabolic dunes under differing wind directions are likely to show a more rounded parabolic morphology [*Pye*,

1982; *Pye and Tsoar*, 1990]. Angularity in dunes could be reduced if avalanches were programmed to function with additional neighboring cells. Also, more realistic stabilized dune profiles could occur if the angle of repose was increased with vegetation cover as in *Nield and Baas* [2008a, 2008b], or included surface moisture [*Nield*, 2011]. We also acknowledge that real climate varies much more than our binary simulation. Other workers have simulated much more complicated stabilization sequences [see *Nield and Baas*, 2008b]. However, we have deliberately kept the model and simulations as simple as possible to facilitate identification of the generic behaviors present in stabilizing dune fields. For example, as a result of holding sediment flux and sediment transport constant, we were forced to pick a value for Q_{max}. We expect further studies to expand upon our results with more detailed boundary conditions and model parameterizations that are specific to certain dune fields.

5.2. Growth of Bare Dunes

[31] The growth of bare dunes from a flat bed is the result of an instability between sediment transport and shear stress documented for similar models by *Werner* [1995], *Pelletier* [2009], *Pelletier et al.* [2009], *Bo and Zheng* [2011], and *Eastwood et al.* [2011]. Small perturbations in the surface brought about by random ordering of transport events form small slipfaces, which advance downwind at a slower rate (proportional to the inverse of slipface height) [*Bagnold*, 1941]. This creates a positive feedback: sediment in transport that encounters an incipient dune will add to the size of the dune, further slowing the dune and increasing the quantity of sediment that encounters the stoss of the dune. Once dunes increase in size, they self-organize through a series of dune-dune interactions, which can be classified as constructive (increasing organization and size), or destructive (decreasing organization and size) (see review by *Kocurek et al.* [2010]). Most interactions in this (and similar)

models are constructive. As time progresses dunes increase in i) height, ii) organization (fewer crest terminations), and iii) spacing [*Werner*, 1995; *Bishop et al.*, 2002; *Eastwood et al.*, 2011] (see Animations S1–S3). These findings have been confirmed to exist in real dune fields [*Ewing et al.*, 2006; *Ewing and Kocurek*, 2010a, 2010b; *Derickson et al.*, 2008; *Elbelrhiti*, 2012].

[32] EST provides a limitation to dune height growth. In simulations, dune height increased with time until the dune troughs encountered non-erodible basement. Subsequent dune growth could only occur with dune collisions and mergers, which tended to increase height at a slower rate. Thus, the largest dunes were associated with greater EST and old growth times (see Figure 4). Although, our model captures the basic interactions that dominate the height development of dunes under simple boundary conditions, we note that other models have shown more complex behavior associated with different boundary conditions [e.g., *Diniega et al.*, 2010].

[33] Although the genesis of dunes from a flat bed is qualitatively understood [*Eastwood et al.*, 2011], the precise timescales of dune genesis are unknown. The development of an incipient slipface from a flat bed is intricately linked with stochasticity in transport, which is suppressed in many dune models [e.g., *Durán and Herrmann*, 2006]. The BAM includes stochasticity by calculating sediment transport and moving sediment with random ordering in the model space. Given this simple approach, fully developed dunes can evolve in timescales ≈75 a. Similar to *Werner* [1995] the genesis of dunes may not be simulated perfectly. Some dune fields could take much longer to develop if transport was less or, stochasticity in transport events was different. Spatiotemporal variability in transport is widely acknowledged to be pervasive at minute to second timescales [see *Baas and Sherman*, 2005, 2006; *Ellis et al.*, 2011]. Presumably some of this variability extends to larger scales, but to our knowledge has yet to be presented in a comprehensive manner (although see promising work by *Dong et al.* [2011]). Further empirical research examining dune genesis is a high priority in aeolian geomorphology.

[34] With the combined effects of pre-stabilization growth time and EST, the pre-stabilization configuration of dunes can vary substantially, from small isolated barchan dunes to large transverse dunes (Figure 4). Vegetation interacts differently with different types of dune topography, yielding different stabilization rates. Our results show three basic behaviors that exert influence on the stabilization rate: i) dune height, ii) dune-dune collisions, and iii) organization and spacing.

5.3. Dune Height Decreases Stabilization Time

[35] The height of dunes is inversely correlated with celerity [*Bagnold*, 1941]; and as a result, height is also inversely correlated with the characteristic rates of topographic change on a dune. Thus, large (slow) dunes were more likely to have topographic change values that could support vegetation (zones (ii) and (iii); Figure 2), and smaller dunes were more likely to have topographic change values that were inhospitable for vegetation (zones (i) and (iv); Figure 3). This scaling has important implications for determining whether a dune will continue to advance under the influence of vegetation (and prolong stabilization).

[36] Downwind dune advance was largely limited by whether or not vegetation grew on the slipface. This is because growth curves only grow vegetation in regions of deposition (Figure 3). Most deposition on dunes is on the slipface. Positive vegetation growth in regions of deposition is supported by biological study [*Maun*, 1998], and observations of real parabolic dunes which commonly show preferential growth of vegetation in regions of deposition [*Pye*, 1982; *Pye and Tsoar*, 1990; *Durán et al.*, 2008]. If vegetation grew on the slipface, it encroached the dune crest and upper stoss, subsequently resulting in stabilization.

[37] We describe slipface vegetation here, but the general trend of larger dunes having lower characteristic topographic change is consistent for all dunes. As the BAM has higher vegetation growth in regions with less topographic change, larger dunes vegetate faster. Simulation results match this: by plotting pre-stabilization dune field height and stabilization time, there is a pronounced increase in stabilization time associated with moderate-sized dunes (Figure 7). A potential real example of massive dunes that stabilized with little form modification is the barchan and transverse dunes found in the Nebraska Sand Hills of USA.

5.4. Dune-Dune Collisions Decrease Stabilization Time

[38] Collisions between dunes tended to accelerate the stabilization process. By collisions we mean situations where a dune overrides all or part of another dune. As dunes collided the upwind dune slowed sufficiently to allow vegetation to encroach. Some dunes survived collisions, particularly with the lower vegetation growth rate of the C1 growth curve, but most stabilized quickly. Collisions provide some explanation for the lower stabilization times observed in dune fields with higher sediment supplies. The well-established relation between pre-stabilization dune field growth time and dune spacing [see *Eastwood et al.*, 2011; *Ewing and Kocurek*, 2010b] regulated the probability of collisions. Dunes that were further apart were less likely to collide.

[39] Collisions also demonstrate the importance of simulating stabilization with models that consider dune morphodynamics and topography. The size and configuration of active patches is determined overwhelmingly by the configuration of dunes in the dune field prior to stabilization. Simpler approaches [e.g., *Yizhaq et al.*, 2007, 2009; *Bailey*, 2011] may not capture these dynamics. Simulating stabilization with single dunes [e.g., *Durán and Herrmann*, 2006] ignores dune-dune collisions and is likely to simulate stabilization times longer than would occur in full dune field simulations.

5.5. Spacing and Organization Modulate Stabilization Time

[40] The number of crest terminations, or 'organization' of the dune field, also controlled the stabilization time. Crest terminations were often the first portion of a dune field to stabilize, triggering a feedback where the dune changed morphology to parabolic. This is because crest terminations either i) were low enough to stabilize because topographic change was low enough to support vegetation, or ii) tended to rotate brinklines downwind (e.g., as barchan horns). Wind-parallel rotation of brinklines resulted in slower
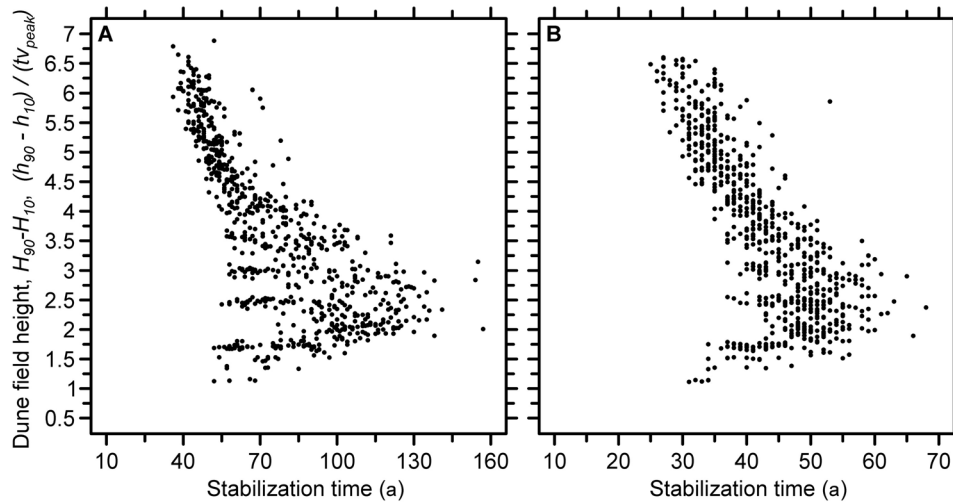
Figure 7. Pre-stabilization dune field height versus stabilization time for the (a) C1 climate shift, and (b) C2 climate shift. Dune field height was calculated by subtracting the 90% and 10% quantiles of the elevation in the model at the instant vegetation was introduced (see Notation).

topographic change because the angle of the dune is more parallel to the downwind vector of dune form movement.

[41] Dunes approaching from upwind that collided with the stabilized crest termination also tended to stabilize. Thus, in a field of transverse or large barchan dunes, the crest terminations acted like stabilization nuclei. Although all dune fields stabilized in the simulations run for this study, previous simulations with a lower growth rate resulted in an unrealistic morphology where one transverse dune spanned the model space. With no crest termination to initiate stabilization, these dune fields were unlikely to ever stabilize. Although this is a model artifact associated with the periodic boundaries, it does demonstrate an extreme case where a perfectly organized dune field can be extremely resistant to stabilizing climate shifts.

5.6. Predicting Relative Stabilization Time From Characteristic Deposition Rates

[42] Although we have cast stabilization time as a function of un-vegetated dune field development time (pre-stabilization growth time) and EST, it could be helpful to examine some alternate methods of characterizing the dune field geomorphology. Although EST can be measured [see *Hugenholtz and Barchyn*, 2010], the pre-stabilization growth time is often difficult to determine conclusively. As discussed in section 5.2, the genesis of dunes is likely not simulated perfectly in the BAM. Further, many natural dune fields do not have an unimpeded development time; there could have been multiple stabilization and activation sequences in the past. It would be helpful to explore a potential method for directly relating the present geomorphology of a dune field with stabilization time.

[43] A host of issues exist with quantifying the geomorphology of dune fields in an objective and robust manner [*Hugenholtz et al.*, 2012, section 3.3; *Baas and Nield*, 2010]. Most methods only quantify the static pattern [e.g., *Ewing et al.*, 2006], rather than some measurement of the kinematics of the dune field. Some measurement of the celerity of dunes is essential to compare with vegetation growth rate

[see *Reitz et al.*, 2010; *Jerolmack et al.*, 2012]. *Durán and Herrmann* [2006] (also *Reitz et al.* [2010] and *Jerolmack et al.* [2012]) successfully used a comparison of the 'total surface change' and 'vertical vegetation growth rate' to describe the susceptibility of individual dunes to transition from barchan to parabolic morphology. However, we propose that the most reliable metric of dune field kinematics is the distribution of deposition rates for the following reasons: i) deposition rates are not susceptible to variability in stoss slope profile, ii) vegetation can begin growing on the slipface, which assumes an (almost) constant slope $\approx 34°$, allowing more robust comparison across dune fields and simple treatment with basic geometry, and iii) deposition rates can be directly compared with the real peak deposition tolerance of vegetation (v_{peak}).

[44] Deposition rates on real dunes can be determined through a number of methods. Most reliably, deposition rates on real dunes can be empirically measured with repeat high resolution topographic surveys [see, e.g., *Hugenholtz*, 2010; *Ewing and Kocurek*, 2010b; *Reitz et al.*, 2010; *Jerolmack et al.*, 2012]. However, deposition rates ($\delta h / \delta t_{depo}$) can also be approximated with equations used to calculate standard yearly streamwise sediment flux (q, in kg m^{-1} a^{-1}) and consideration of slipface geometry with

$$\delta h / \delta t_{depo} \approx q / \left(\rho_{bulk} h_{slipface} \right) \cdot \sin(\Phi) \cdot \tan\left(\theta_{repose} \right) \qquad (4)$$

where ρ_{bulk} is the bulk density of sediment when deposited in the dune, $h_{slipface}$ is the height of the slipface, Φ is the brinkline angle relative to sediment transport, and θ_{repose} is the angle of repose. Note that this method requires the assumption that most deposition in a dune field is on the slipface. Representative values for v_{peak} could also be extracted from remote sensing records by comparing measured deposition rates with the presence or absence of vegetation on dune slipfaces. On our modeled dunes, we quantify deposition rates by examining the difference between topography at a given time and topography one time interval t
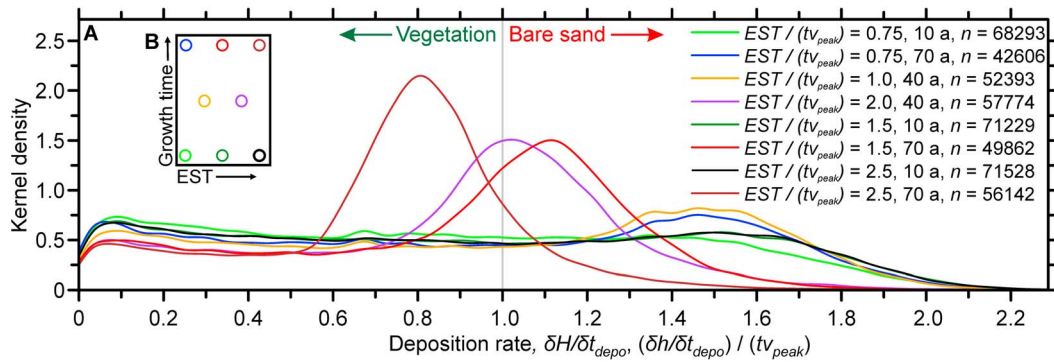
Figure 8. Distribution of deposition rates for various dune fields at the instant vegetation was introduced (model values: $\delta H/\delta t_{depo}$, real values: $\delta h/\delta t_{depo}/(t v_{peak})$). (a) Deposition rates are pooled for the ten simulations with parameters listed, n = number of measurements available, kernel density bandwidth = 0.03. (b) Color-coded inset gives a visual representation of the relative positioning of each curve within the phase-space of simulations. Note: portions of the distribution where $\delta H/\delta t_{depo} < 1.0$ (or $(\delta h/\delta t_{depo}/(t v_{peak})) < 1.0$) support vegetation on the slipface of dunes, and represent environments that are likely to trend toward stabilization. The relative proportion of deposition environments in real dune fields above and below 1.0 could provide an indicator of relative stabilization time.

prior. All cells that have positive balance (deposition) are extracted for analysis.

[45] In a dune field there will be a range of deposition values because there is a range of dune sizes and brinkline orientations (see Figure 8). This distribution could be used to develop a quantitative predictor of the relative stabilization time as the values can be directly compared with v_{peak}. Portions of the distribution where $\delta h/\delta t_{depo} > v_{peak}$ will advance unimpeded without growing vegetation on the slipface of the dune. Contrarily, areas where $\delta h/\delta t_{depo} < v_{peak}$ will support vegetation growth on the slipface. In our simulated dunes, this vegetation reaches the upper crest as the dune advances, eventually trending that dune to stabilization; further research is required to ascertain if this behavior is as predictable in real dunes. With this simplification, the distribution of $\delta h/\delta t_{depo}$ can be classified into two types of environments in our simulated dunes: areas that support vegetation growth and those that do not. The relative proportion of each environment in the dune field and distribution of $\delta h/\delta t_{depo}$ can be used to provide a predictor of the relative proportion of the dune field that advances unimpeded by vegetation, and the proportion that begins a feedback toward stabilization. This distribution varies with different dune field geomorphologies (Figure 8).

[46] To facilitate more rigorous analysis, we calculated several metrics of the $\delta h/\delta t_{depo}$ distribution: i) $\delta h/\delta t_{depo\ q75}$: the 75% quantile of deposition rates, ii) $\delta h/\delta t_{depo\ q75} - \delta h/\delta t_{depo\ q25}$: the difference between the 75% and 25% quantiles of deposition rate, and iii) r_{vpeak}: the quantile of $\delta h/\delta t_{depo}$ that equals v_{peak}, which is equivalent to the relative proportion of deposition environments that have deposition rates less than v_{peak} (and will support vegetation growth). These distributions can be compared with pre-stabilization growth time and EST (Figure 9), or with the stabilization time (Figure 10).

[47] Under both the C1 and C2 vegetation growth regimes, reasonably well defined relations between the deposition metrics and stabilization time exist (Figure 10). A positive correlation exists between $\delta h/\delta t_{depo\ q75}$ and stabilization

time: environments with the 75% quantile of deposition rate that fall below v_{peak} are destined to stabilize quickly. A positive correlation exists between $\delta h/\delta t_{depo\ q75} - \delta h/\delta t_{depo\ q25}$ and stabilization time: this suggests that dune fields that had prolonged stabilizations also had a large spread in the distribution of deposition rates. A portion of this result may be caused by measurement artifacts around dune crests where a net change of zero elevation is recorded in some locations as the dune crest passes partway through the measurement interval. However, a large spread in deposition rates is also found with crest terminations, whose brinkline rotation reduces characteristic values of $\delta h/\delta t_{depo}$ as per equation (4). Barchan dune fields, with many crest terminations, could have considerable portions of the $\delta h/\delta t_{depo}$ distribution that is less than v_{peak} due to brinkline rotation. Finally, comparing r_{vpeak} with stabilization time shows a weak negative correlation suggesting that r_{vpeak} is a less robust predictor of relative stabilization time. Overall, stronger relations exist with the C2 vegetation growth regime, suggesting that relative dune field stabilization time may be more predictable with higher vegetation growth rates. In all cases, when the distribution of $\delta h/\delta t_{depo}$ shifted toward higher values relative to v_{peak} the spread in results increased; which could be attributed to greater potential for collisions and variability in spatial configuration of dunes (see sections 5.4 and 5.5).

[48] In general, comparing the deposition rates in a dune field to v_{peak} should provide a reasonably robust predictor of the relative stabilization time. The deposition rate metrics in Figures 8, 9, and 10 are likely to be widely applicable and directly comparable to measurements made in real dune fields. We expect the general linear relations in Figure 10 will hold within the ranges shown if vegetation growth regime is similar in configuration to Figure 3. However, we are less confident with the precise slope of linear predictions (Figure 10).

[49] Several factors suggest that precise prediction of the absolute stabilization time could be difficult. First, different slopes are seen with the C1 and C2 growth regimes
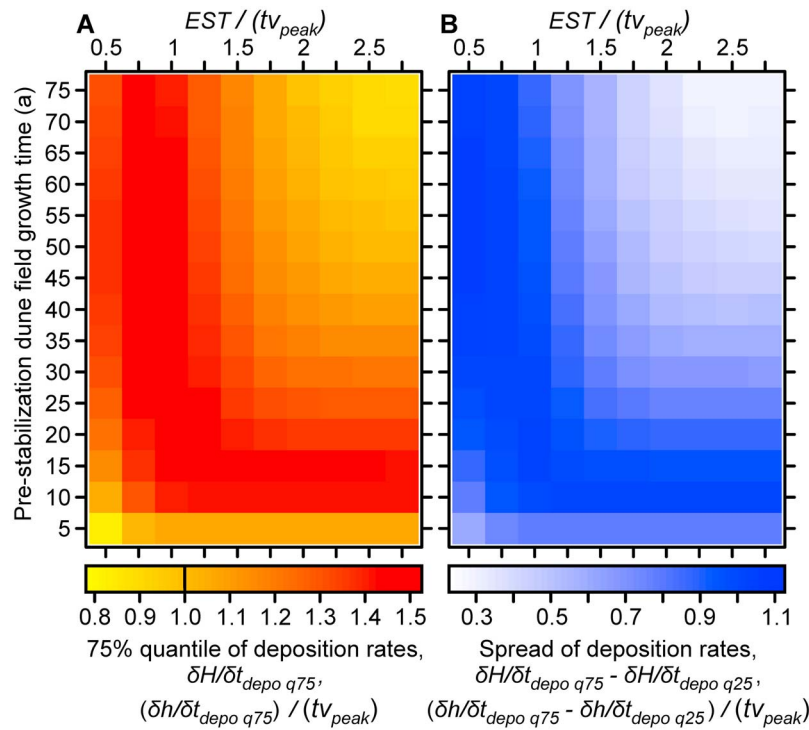
Figure 9. Metrics of the distribution of deposition rate plotted against pre-stabilization growth time and equivalent sediment thickness ($EST \cdot \alpha$) for all simulations without vegetation. (a) 75% quantile of deposition rate distribution. (b) Spread of deposition rates (75% - 25% quantiles). Note: metrics can be represented as model values (e.g., $\delta H / \delta t_{depo}$) or real values (e.g., $\delta h / \delta t_{depo} / (tv_{peak})$) (see Notation).

(Figure 10), which suggests the rate of stabilization of a given portion of a dune is extremely sensitive to the vegetation growth magnitude. Second, additional sub-gridcell scale processes not incorporated into the BAM could influence the rate of stabilization. For example, the formation of nebkhas on the crest of dunes could modify results in poorly understood manners [e.g, *Ardon et al.*, 2009]. Furthermore, significant uncertainty exists with the response of vegetation growth to topographic change (see section 2). *Nield and Baas* [2008b] outlined considerable complexity in the stabilization and activation sequences of dune fields that were developed with multiple activation and stabilization cycles. This could produce distributions of deposition rates that differ from our results. Despite these difficulties, comparing the distribution of deposition rates to v_{peak} does show promise in its simplicity and use of measurements that are straightforward to determine for many dune fields.

6. Approaches to Compare Simulated Results With Real Dunes

[50] Simulations with the BAM suggest that the stabilization rate of dune fields imposed by climate is modified by the geomorphology of the dune field. These findings have not been previously identified. As noted in section 2, considerable uncertainties exist in predictions from all numerical dune field models. Fortunately, there are several readily available methods to qualitatively and quantitatively explore the robustness of our results in *real* dune fields.

[51] Assuming identical dune growth time and applied to a large dune field, areas with less EST should stabilize first, followed by areas with greater EST and those with moderate EST. If there is variability in growth time, the younger portions of the dune field are likely to stabilize first, followed by older portions of the dune field. The influence of growth time is reversed if the EST is greater, albeit much less pronounced, as portions of the dune field with greater pre-stabilization growth time are likely to stabilize first, followed by those which are younger. The ranges in stabilization rate indicate that portions of dune fields could remain active much longer than other portions, and these differences may be substantial. This is commonly seen in stabilizing dune fields. For example dunes in southwestern Saskatchewan, Canada are largely stabilized except for a few isolated dunes that have managed to maintain activity far longer than nearby dunes [see *Hugenholtz and Wolfe*, 2005a; *Wolfe and Hugenholtz*, 2009; *Hugenholtz*, 2010]. Dune stabilization chronologies can be accurately and directly dated with well-established optical dating procedures [e.g., *Wolfe and Hugenholtz*, 2009].

[52] Dune fields with pronounced differences in EST and growth time are common [see *Kocurek and Ewing*, 2005; *Ewing et al.*, 2006]. For example, dune fields forming from a beach often transfer sand inland and steadily increase in growth time away from the coast (see Figure 11) [*Ewing and Kocurek*, 2010b]. Differences in EST vary across many dune fields, governed by local sediment supply and the evolution of the dune field [*Wasson and Hyde*, 1983]. Aspects of growth time (such as spacing and number of crest
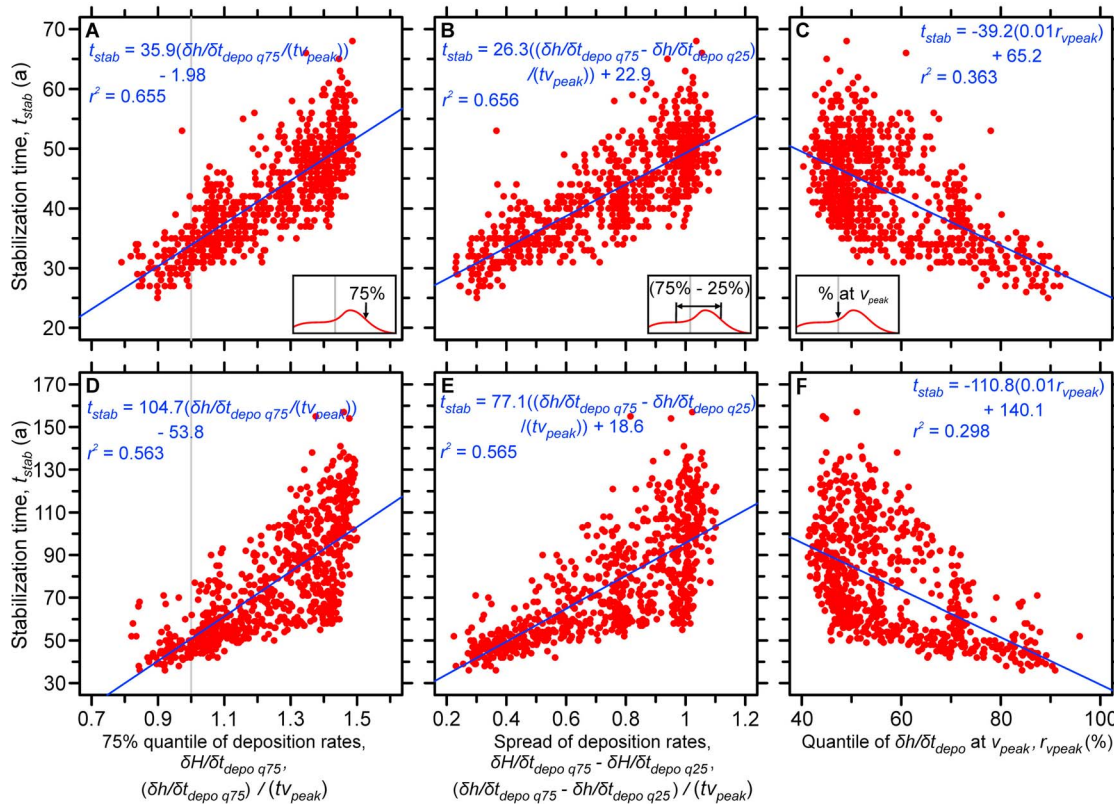
Figure 10. Metrics of the distribution of deposition rate at the instant vegetation was introduced plotted against stabilization time. For vegetation growth regime C2: (a) 75% quantile of deposition rate versus stabilization time, (b) spread of deposition rates versus stabilization time, (c) The quantile of the deposition rate distribution corresponding to the peak deposition tolerance of vegetation (v_{peak}). For vegetation growth regime C1: (d) 75% quantile of deposition rate versus stabilization time, (e) spread of deposition rates versus stabilization time, (f) The quantile of the deposition rate distribution corresponding to the peak deposition tolerance of vegetation (v_{peak}). Note: metrics can be represented as model values (e.g., $\delta H/\delta t_{depo}$) or real values (e.g., $\delta h/\delta t_{depo}/(tv_{peak})$) (see Notation). Small insets in Figures 10a–10c are guides to help represent values on horizontal axis of plots.

terminations) can be mapped through techniques presented by *Ewing and Kocurek* [2010a, 2010b]. EST can also be approximated with GIS techniques such as those presented by *Hugenholtz and Barchyn* [2010]. With these techniques, dune fields could be directly monitored during stabilization.

[53] Direct quantitative testing of presently active dune fields may be best performed by comparison of characteristic deposition rates and v_{peak} (section 5.6). This can be directly measured for a dune field by either i) repeat high resolution topographic surveys [e.g., *Hugenholtz*, 2010; *Reitz et al.*, 2010; *Jerolmack et al.*, 2012], or ii) inference from process based equations and equation (4). An estimate for v_{peak} could be developed from plot experiments [e.g., *Maun and Perumal*, 1999] or through remote sensing by combining estimates of deposition with imagery to track sites where deposition is high enough to completely bury vegetation. With these two values, the distribution of $\delta h/\delta t_{depo}$ could be plotted in Figures 8, 9, 10, and compared with simulated values. This would provide a quantitatively based prediction of the relative stabilization time, allowing researchers to hypothesize whether a given dune field is likely to prolong stabilization, or stabilize almost immediately. To

aid researchers who wish to compare results with our simulations we have provided 4 supplementary data sets tracking the stabilization of dune fields shown in Figure 5 (Data Sets S1–S3), and an overview of dune field characteristics as related to stabilization time (Data Set S4).

7. Implications and Conclusions

[54] Overall, our simulations indicate that spatial variations in the configuration of dune fields can create a mosaic of different stabilization rates under the same climate forcing. The spatial heterogeneity of stabilization could explain the observed bistability of dune fields in many coastal and inland locations, while also accounting for observed lags between dune field activity and climate [e.g., *Miao et al.*, 2007; *Wolfe and Hugenholtz*, 2009]. This potentially has major implications for research involving paleoenvironmental reconstruction and prediction of dune field activity. Many studies relate stratigraphic proxies to periods of dune field activity or stability and infer 1:1 correspondence to external drivers such as climate.

[55] Our findings suggest that the response of dune fields to major climate forcings can be modulated by their
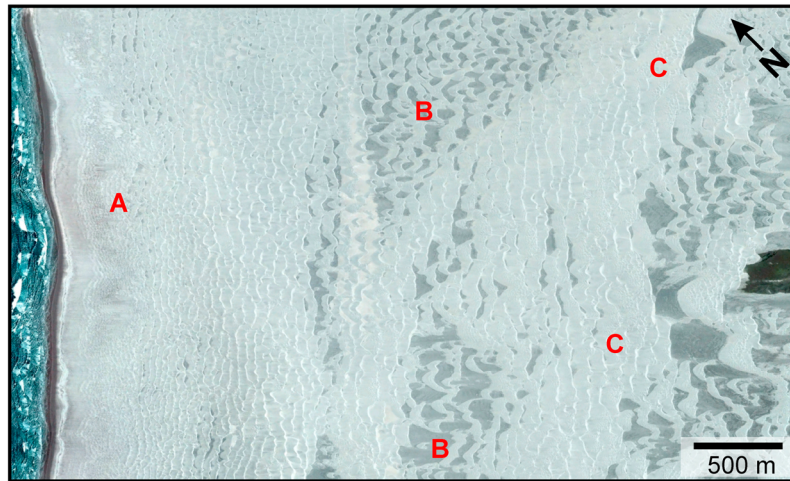
Figure 11. Dune fields naturally vary in geomorphology: an example from Guerrero Negro, BCS, México (27.937365° N, 114.232270° W). If this dune field were subject to a climate shift where vegetation began to stabilize the dunes, our results suggest different parts of this dune field may behave differently. (a) Dunes adjacent to the coastline appear to be young and immature and are likely to stabilize quickly. (b) Dunes further inland are moderate sized and wider spaced; these dunes could cushion the increase in vegetation by forming parabolic dunes. (c) Large and well-organized transverse dunes further inland could stabilize quickly.

geomorphology. Significant lags may exist. Thus, dune field stabilization rate should not be viewed exclusively in the context of climate.

Notation

EST real equivalent sediment thickness, m

B model basement elevation (always = 0), non-dimensional

b real basement elevation (always = 0), m

D_{fetch} maximum fetch distance in model, cells

D_{upwind} distance upwind from the focal cell in model, cells

$\delta H/\delta t_{depo}$ deposition rates in a model dune field, a^{-1}

$\delta H/\delta t_{depo\ q75}$ 75% quantile of deposition rates in a modeled dune field, a^{-1}

$\delta H/\delta t_{depo\ q25}$ 25% quantile of deposition rates in a modeled dune field, a^{-1}

$\delta h/\delta t_{depo}$ deposition rates in a real dune field, m a^{-1}

$\delta h/\delta t_{depo\ q75}$ 75% quantile of deposition rates in a real dune field, m a^{-1}

$\delta h/\delta t_{depo\ q25}$ 25% quantile of deposition rates in a real dune field, m a^{-1}

H model elevation measurement, non-dimensional

H_{90} 90% quantile of model elevation, non-dimensional

H_{10} 10% quantile of model elevation, non-dimensional

h real elevation measurement, m

h_{90} 90% quantile of real elevation, m

h_{10} 10% quantile of real elevation, m

$h_{slipface}$ real slipface height, m

l_{model} model length measurement, non-dimensional

l_{real} real length measurement, m

Φ planform brinkline angle measured from wind direction, °

Q model sediment flux, per transport event

q real sediment flux, kg m^{-1} a^{-1}

Q_{max} model maximum (saturated) sediment flux, constant at 0.1 per transport event

q_{max} real maximum (saturated) yearly sediment flux, m^2 a^{-1}

ρ_{bulk} bulk density of sediment when deposited in the dune, kg m^{-3}

r_{vpeak} quantile of $\delta h/\delta t_{depo}$ that equals v_{peak}, %

t time unit used to measure v_{peak} (constant at 1 a), a

t_{stab} stabilization time, a

τ surface shear stress from wind

θ_{repose} angle of repose, °

V model vegetation cover

v real vegetation cover, % of real cell size

$v_{shelter}$ real vegetation cover that results in cessation of transport, % of real cell size

V_{peak} model maximum rate of deposition vegetation can survive (constant at 1 a^{-1}), a^{-1}

v_{peak} real maximum rate of deposition vegetation can survive, m a^{-1}

References

Anthonsen, K. L., L. B. Clemmensen, and J. H. Jensen (1996), Evolution of a dune from crescentic to parabolic form in response to short-term climatic changes: Råbjerg Mile, Skagen Odde, Denmark, *Geomorphology*, *17*, 63–77, doi:10.1016/0169-555X(95)00091-I.

Ardon, K., H. Tsoar, and D. G. Blumberg (2009), Dynamics of nebkhas superimposed on a parabolic dune and their effect on the dune dynamics, *J. Arid Environ.*, *73*, 1014–1022, doi:10.1016/j.jaridenv.2009.04.021.

Ash, J. E., and R. J. Wasson (1983), Vegetation and sand mobility in the Australian desert dune field, *Z. Geomorphol.*, *45*, 7–25.

Baas, A. C. W. (2002), Chaos, fractals and self-organization in coastal geomorphology: Simulating dune landscapes in vegetated environments, *Geomorphology*, *48*, 309–328, doi:10.1016/S0169-555X(02)00187-3.

Baas, A. C. W. (2007), Complex systems in aeolian geomorphology, *Geomorphology*, *91*, 311–331, doi:10.1016/j.geomorph.2007.04.012.

Baas, A. C. W., and J. M. Nield (2007), Modelling vegetated dune landscapes, *Geophys. Res. Lett.*, *34*, L06405, doi:10.1029/2006GL029152.

Baas, A. C. W., and J. M. Nield (2010), Ecogeomorphic state variables and phase-space construction for quantifying the evolution of vegetated aeolian landscapes, *Earth Surf. Processes Landforms*, *35*, 717–731, doi:10.1002/esp.1990.

Baas, A. C. W., and D. J. Sherman (2005), Formation and behavior of aeolian streamers, *J. Geophys. Res.*, *110*, F03011, doi:10.1029/2004JF000270.

Baas, A. C. W., and D. J. Sherman (2006), Spatiotemporal variability of aeolian sand transport in a coastal dune environment, *J. Coastal Res.*, *22*, 1198–1205, doi:10.2112/06-0002.1.

Bagnold, R. A. (1941), *The Physics of Blown Sand and Desert Dunes*, Methuen, London.

Bailey, R. M. (2011), Spatial and temporal signatures of fragility and threshold proximity in modelled semi-arid vegetation, *Proc. R. Soc. B*, *278*, 1064–1071, doi:10.1098/rspb.2010.1750.

Bailey, S. D., and C. S. Bristow (2004), Migration of parabolic dunes at Aberffraw, Anglesey, north Wales, *Geomorphology*, *59*, 165–174, doi:10.1016/j.geomorph.2003.09.013.

Bishop, S. R., H. Momiji, R. Carretero-Gonzáles, and A. Warren (2002), Modelling desert dune fields based on discrete dynamics, *Discrete Dyn. Nat. Soc.*, *7*, 7–17, doi:10.1080/10260220290013462.

Bo, T.-L., and X.-J. Zheng (2011), The formation and evolution of aeolian dune fields under unidirectional wind, *Geomorphology*, *134*, 408–416, doi:10.1016/j.geomorph.2011.07.014.

Bowers, J. E. (1982), The plant ecology of inland dunes in western North America, *J. Arid Environ.*, *5*, 199–220.

Brown, J. F. (1997), Effects of experimental burial on survival, growth, and resource allocation of three species of dune plants, *J. Ecol.*, *85*, 151–158, doi:10.2307/2960647.

Bullard, J. E., D. S. G. Thomas, I. Livingstone, and G. F. S. Wiggs (1997), Dune field activity and interactions with climatic variability in the southwest Kalahari Desert, *Earth Surf. Processes Landforms*, *22*, 165–174, doi:10.1002/(SICI)1096-9837(199702)22:2<165::AID-ESP687>3.0.CO;2-9.

Chase, B. (2009), Evaluating the use of dune sediments as a proxy for palaeo-aridity: A southern African case study, *Earth Sci. Rev.*, *93*, 31–45, doi:10.1016/j.earscirev.2008.12.004.

Chase, B. M., and D. S. G. Thomas (2006), Late Quaternary dune accumulation along the western margin of South Africa: Distinguishing forcing mechanisms through the analysis of migratory dune forms, *Earth Planet. Sci. Lett.*, *251*, 318–333, doi:10.1016/j.epsl.2006.09.017.

de Castro, F. (1995), Computer simulation of the dynamics of a dune system, *Ecol. Modell.*, *78*, 205–217, doi:10.1016/0304-3800(93)E0090-P.

Dech, J. P., and M. A. Maun (2005), Zonation of vegetation along a burial gradient on the leeward slopes of Lake Huron sand dunes, *Can. J. Bot.*, *83*, 227–236, doi:10.1139/b04-163.

Delgado-Fernandez, I. (2010), A review of the application of the fetch effect to modelling sand supply to coastal foredunes, *Aeolian Res.*, *2*, 61–70, doi:10.1016/j.aeolia.2010.04.001.

de M. Luna, M. C. M., E. J. R. Parteli, O. Durán, and H. J. Herrmann (2011), Model for the genesis of coastal dune fields with vegetation, *Geomorphology*, *129*, 215–224, doi:10.1016/j.geomorph.2011.01.024.

Derickson, D., G. Kocurek, R. C. Ewing, and C. Bristow (2008), Origin of a complex and spatially diverse dune-field pattern, Algodones, southeastern California, *Geomorphology*, *99*, 186–204, doi:10.1016/j.geomorph.2007.10.016.

Diniega, S., K. Glasner, and S. Byrne (2010), Long-time evolution of models of aeolian sand dune fields: Influence of dune formation and collision, *Geomorphology*, *121*, 55–68, doi:10.1016/j.geomorph.2009.02.010.

Dong, Z., Z. Zhang, P. Lü, and G. Qian (2011), An aeolian transport model for flat shifting sand fields under dynamic-limiting conditions, *J. Arid Environ.*, *75*, 865–869, doi:10.1016/j.jaridenv.2011.03.012.

Durán, O., and H. J. Herrmann (2006), Vegetation against dune mobility, *Phys. Rev. Lett.*, *97*, 188001, doi:10.1103/PhysRevLett.97.188001.

Durán, O., M. V. N. Silva, L. J. C. Bezerra, H. J. Herrmann, and L. P. Maia (2008), Measurements and numerical simulations of the degree of activity and vegetation cover on parabolic dunes in north-eastern Brazil, *Geomorphology*, *102*, 460–471, doi:10.1016/j.geomorph.2008.05.011.

Eastwood, E., J. M. Nield, A. C. W. Baas, and G. Kocurek (2011), Modelling controls on aeolian dune-field pattern evolution, *Sedimentology*, *58*, 1391–1406, doi:10.1111/j.1365-3091.2010.01216.x.

Elbelrhiti, H. (2012), Initiation and early development of barchan dunes: A case study of the Moroccan Atlantic Sahara desert, *Geomorphology*, *138*, 181–188, doi:10.1016/j.geomorph.2011.08.033.

Ellis, J. T., D. J. Sherman, E. J. Farrell, and B. Li (2011), Temporal and spatial variability of aeolian sand transport: Implications for field measurements, *Aeolian Res*, *3*, 379–387.

Ewing, R. C., and G. Kocurek (2010a), Aeolian dune interactions and dune-field pattern formation: White Sands Dune field, New Mexico, *Sedimentology*, *57*, 1199–1219.

Ewing, R. C., and G. Kocurek (2010b), Aeolian dune-field pattern boundary conditions, *Geomorphology*, *114*, 175–187, doi:10.1016/j.geomorph.2009.06.015.

Ewing, R. C., G. Kocurek, and L. W. Lake (2006), Pattern analysis of dune-field parameters, *Earth Surf. Processes Landforms*, *31*, 1176–1191, doi:10.1002/esp.1312.

Forman, S. L., R. Oglesby, and R. S. Webb (2001), Temporal and spatial patterns of Holocene dune activity on the Great Plains of North America: Megadroughts and climate links, *Global Planet. Change*, *29*, 1–29, doi:10.1016/S0921-8181(00)00092-8.

Frank, A., and G. Kocurek (1996), Toward a model for airflow on the lee side of aeolian dunes, *Sedimentology*, *43*, 451–458, doi:10.1046/j.1365-3091.1996.d01-20.x.

Franks, S. J., and C. J. Peterson (2003), Burial disturbance leads to facilitation among coastal dune plants, *Plant Ecol.*, *168*, 13–21, doi:10.1023/A:1024450623205.

Hugenholtz, C. H. (2010), Topographic changes of a supply limited inland parabolic sand dune during the incipient phase of stabilization, *Earth Surf. Processes Landforms*, *35*, 1674–1681, doi:10.1002/esp.2053.

Hugenholtz, C. H., and T. E. Barchyn (2010), Spatial analysis of sand dunes with a new global topographic dataset: New approaches and opportunities, *Earth Surf. Processes Landforms*, *35*, 986–992, doi:10.1002/esp.2013.

Hugenholtz, C. H., and S. A. Wolfe (2005a), Biogeomorphic model of dune field activation and stabilization on the northern Great Plains, *Geomorphology*, *70*, 53–70, doi:10.1016/j.geomorph.2005.03.011.

Hugenholtz, C. H., and S. A. Wolfe (2005b), Recent stabilization of active sand dunes on the Canadian prairies and relation to recent climate variations, *Geomorphology*, *68*, 131–147, doi:10.1016/j.geomorph.2004.04.009.

Hugenholtz, C. H., S. A. Wolfe, I. J. Walker, and B. J. Moorman (2009), Spatial and temporal patterns of aeolian sediment transport on an inland parabolic dune, Bigstick Sand Hills, Saskatchewan, Canada, *Geomorphology*, *105*, 158–170, doi:10.1016/j.geomorph.2007.12.017.

Hugenholtz, C. H., N. Levin, T. E. Barchyn, and M. C. Baddock (2012), Remote sensing and spatial analysis of aeolian sand dunes: A review and outlook, *Earth Sci. Rev.*, *111*, 319–334, doi:10.1016/j.earscirev.2011.11.006.

Jerolmack, D. J., R. C. Ewing, F. Falcini, R. L. Martin, C. Masteller, C. Phillips, M. D. Reitz, and I. Buynevich (2012), Internal boundary layer model for the evolution of desert dune fields, *Nat. Geosci.*, *5*, 206–209, doi:10.1038/ngeo1381.

Kocurek, G., and R. C. Ewing (2005), Aeolian dune field self-organization– implications for the formation of simple versus complex dune-field patterns, *Geomorphology*, *72*, 94–105, doi:10.1016/j.geomorph.2005.05.005.

Kocurek, G., R. C. Ewing, and D. Mohrig (2010), How do bedform patterns arise? New views on the role of bedform interactions within a set of boundary conditions, *Earth Surf. Processes Landforms*, *35*, 51–63, doi:10.1002/esp.1913.

Laity, J. (2003), Aeolian destabilization along the Mojave River, Mojave Desert, California: Linkages among fluvial, groundwater, and aeolian systems, *Phys. Geog.*, *24*, 196–221, doi:10.2747/0272-3646.24.3.196.

Lancaster, N. (1988), Development of linear dunes in the south-western Kalahari, southern Africa, *J. Arid Environ.*, *14*, 233–244.

Lancaster, N., and A. Baas (1998), Influence of vegetation cover on sand transport by wind: Field studies at Owens Lake, California, *Earth Surf. Processes Landforms*, *23*, 69–82, doi:10.1002/(SICI)1096-9837(199801)23:1<69::AID-ESP823>3.0.CO;2-G.

Marín, L., S. L. Forman, A. Valdez, and F. Bunch (2005), Twentieth century dune migration at the Great Sand Dunes National Park and Preserve, Colorado, relation to drought variability, *Geomorphology*, *70*, 163–183, doi:10.1016/j.geomorph.2005.04.014.

Maun, M. A. (1998), Adaptations of plants to burial in coastal sand dunes, *Can. J. Bot.*, *76*, 713–738, doi:10.1139/b98-058.

Maun, M. A., and J. Perumal (1999), Zonation of vegetation on lacustrine coastal dunes: Effects of burial by sand, *Ecol. Lett.*, *2*, 14–18, doi:10.1046/j.1461-0248.1999.21048.x.

Miao, X., J. A. Mason, J. B. Swinehart, D. B. Loope, P. R. Hanson, R. J. Goble, and X. Liu (2007), A 10,000 year record of dune activity, dust storms, and severe drought in the central Great Plains, *Geology*, *35*, 119–122, doi:10.1130/G23133A.1.

Murray, A. B. (2007), Reducing model complexity for explanation and prediction, *Geomorphology*, *90*, 178–191, doi:10.1016/j.geomorph.2006.10.020.

Nield, J. M. (2011), Surface moisture-induced feedback in aeolian environments, *Geology*, *39*, 915–918, doi:10.1130/G32151.1.

Nield, J. M., and A. C. W. Baas (2008a), Investigating parabolic and nebkha dune formation using a cellular automaton modelling approach, *Earth Surf. Processes Landforms*, *33*, 724–740, doi:10.1002/esp.1571.

Nield, J. M., and A. C. W. Baas (2008b), The influence of different environmental and climatic conditions on vegetated aeolian dune landscape development and response, *Global Planet. Change*, *64*, 76–92, doi:10.1016/j.gloplacha.2008.10.002.

Nishimori, H., and H. Tanaka (2001), A simple model for the formation of vegetated dunes, *Earth Surf. Processes Landforms*, *26*, 1143–1150, doi:10.1002/esp.258.

Owen, N. W., M. Kent, and M. P. Dale (2004), Plant species and community responses to sand burial on the machair of the Outer Hebrides, Scotland, *J. Veg. Sci.*, *15*, 669–678, doi:10.1111/j.1654-1103.2004.tb02309.x.

Pelletier, J. D. (2009), Controls on the height and spacing of eolian ripples and transverse dunes: A numerical modeling investigation, *Geomorphology*, *105*, 322–333, doi:10.1016/j.geomorph.2008.10.010.

Pelletier, J. D., H. Mitasova, R. S. Harmon, and M. Overton (2009), The effects of interdune vegetation changes on eolian dune field evolution: A numerical-modeling case study at Jockey's Ridge, North Carolina, USA, *Earth Surf. Processes Landforms*, *34*, 1245–1254, doi:10.1002/esp.1809.

Pye, K. (1982), Morphological development of coastal dunes in a humid tropical environment, Cape Bedford and Cape Flattery, North Queensland, *Geogr. Ann., Ser. A*, *64*, 213–227, doi:10.2307/520647.

Pye, K., and H. Tsoar (1990), *Aeolian Sand and Sand Dunes*, Unwin Hyman, London, doi:10.1007/978-94-011-5986-9.

Reitz, M. D., D. J. Jerolmack, R. C. Ewing, and R. L. Martin (2010), Barchan-parabolic dune pattern transition from vegetation stability threshold, *Geophys. Res. Lett.*, *37*, L19402, doi:10.1029/2010GL044957.

Stone, A. E. C., and D. S. G. Thomas (2008), Linear dune accumulation chronologies from the southwest Kalahari, Namibia: Challenges of reconstructing late Quaternary palaeoenvironments from aeolian landforms, *Quat. Sci. Rev.*, *27*, 1667–1681, doi:10.1016/j.quascirev.2008.06.008.

Thomas, D. S. G., and G. F. S. Wiggs (2008), Aeolian system responses to global change: Challenges of scale, process and temporal integration, *Earth Surf. Processes Landforms*, *33*, 1396–1418, doi:10.1002/esp.1719.

Thomas, D. S. G., M. Knight, and G. F. S. Wiggs (2005), Remobilization of southern African desert dune systems by twenty-first century global warming, *Nature*, *435*, 1218–1221, doi:10.1038/nature03717.

Tsoar, H. (2005), Sand dunes mobility and stability in relation to climate, *Physica A*, *357*, 50–56, doi:10.1016/j.physa.2005.05.067.

Tsoar, H., and D. G. Blumberg (2002), Formation of parabolic dunes from barchan and transverse dunes along Israel's Mediterranean Coast, *Earth Surf. Processes Landforms*, *27*, 1147–1161, doi:10.1002/esp.417.

Wasson, R. J., and R. Hyde (1983), Factors determining desert dune type, *Nature*, *304*, 337–339, doi:10.1038/304337a0.

Wasson, R. J., and P. M. Nanninga (1986), Estimating wind transport of sand on vegetated surfaces, *Earth Surf. Processes Landforms*, *11*, 505–514, doi:10.1002/esp.3290110505.

Werner, B. T. (1995), Eolian dunes: Computer simulations and attractor interpretation, *Geology*, *23*, 1107–1110, doi:10.1130/0091-7613(1995)023<1107:EDCSAA>2.3.CO;2.

Wolfe, S. A., and C. H. Hugenholtz (2009), Barchan dunes stabilized under recent climate warming on the northern Great Plains, *Geology*, *37*, 1039–1042, doi:10.1130/G30334A.1.

Wolfe, S. A., J. Bond, and M. Lamothe (2011), Dune stabilization in central and southern Yukon in relation to early Holocene environmental change, northwestern North America, *Quat. Sci. Rev.*, *30*, 324–334, doi:10.1016/j.quascirev.2010.11.010.

Yizhaq, H., Y. Ashkenazy, and H. Tsoar (2007), Why do active and stabilized dunes coexist under the same climatic conditions?, *Phys. Rev. Lett.*, *98*, 188001, doi:10.1103/PhysRevLett.98.188001.

Yizhaq, H., Y. Ashkenazy, and H. Tsoar (2009), Sand dune dynamics and climate change: A modeling approach, *J. Geophys. Res.*, *114*, F01023, doi:10.1029/2008JF001138.

Zarnetske, P. L., S. D. Hacker, E. W. Seabloom, P. Ruggiero, J. R. Killian, T. B. Madduz, and D. Cox (2012), Biophysical feedback mediates effects of invasive grasses on coastal dune shape, *Ecology*, doi:10.1890/11-1112.1, in press.